Electron tunneling through water layers: Effect of layer structure and thickness

Ilan Benjamin,[a] Deborah Evans,[b] and Abraham Nitzan
School of Chemistry, the Raymond and Beverly Sackler Faculty of Science, Tel Aviv University, Tel Aviv, 69978, Israel

(Received 13 December 1996; accepted 16 January 1997)

The effect of thickness and molecular structure on the probability of electron tunneling through water layers is investigated using a recently developed method. Water configurations of 1–4 layers are prepared between two parallel slabs of the Pt(100) surface, using equilibrium molecular dynamics and the polarizable simple point charge water model. Electron tunneling probabilities through the different water layers are computed as functions of energy using the absorbing boundary conditions Green function method and employing either an effective two-body water–electron interaction or a many-body polarizable water–electron potential. As long as the electron incident energy is below the barrier and far from a resonance state, the tunneling probabilities can be reasonably fitted to a one-dimensional rectangular-barrier model. However, near and over-barrier transmission probabilities cannot be reasonably described using a one-dimensional model, and the three-dimensional discrete structure of the water plays an important role. In all systems, the many-body electronic polarizability of the water significantly affects the transmission probability. The role played by the first adsorbed water layer is also discussed. © *1997 American Institute of Physics.* [S0021-9606(97)50516-2]

I. INTRODUCTION

Electron tunneling through a condensed phase barrier is of fundamental importance to many processes in the physical and biological sciences.[1] One example of recent intense interest is the operation of the scanning tunneling microscope (STM), which has found many applications in electrochemistry, surface science, and biophysics. Despite numerous contributions, our theoretical understanding of the factors that influence the tunneling probability (and thus the tunneling current) is still incomplete. This situation is the result of several approximations and simplifying assumptions. In particular, most theoretical treatments of the tunneling process describe the condensed environment as a dielectric continuum. Consequently, the tunneling processes are usually described using one-dimensional models. Recent numerical studies of electron tunneling through three-dimensional molecularly detailed water structures[2–4] have demonstrated the inadequacy of such models for the quantitative accounting of the tunneling probability: First, elastic and inelastic scattering of the electron by the molecular structure make it impossible to describe the tunneling process using a one-dimensional model. Second, the tunneling probability is strongly dependent on details of the molecular structure, such as the orientation of water molecules relative to the tunneling direction and their structure at the donor and acceptor sites. Finally, particular structures can support quasi-bound states of the electron. In neutral bulk water, such states have been designated as precursor states to electron solvation[5] and similar states are probably supported by interfacial structures, e.g., for water near an electrode surface, or by solutes and other impurities. In the context of electron transmission by water structures, these states may contribute to resonance tunneling and therefore strongly affect the energy dependence and the absolute magnitude of the tunneling probability.[4,6–10] Similarly, ordered molecular structures may also affect electron transmission processes via their underlying band structure.[11,12]

Numerical studies[4] have also shown, as could be expected, that the large sensitivity to the barrier structure makes details of the electron–water interaction quite important in the quantitative understanding of the tunneling process. In particular, the many-body response associated with the polarizable nature of the water molecules may have significant impact on the energy and spatial characteristics of electron ''resonance'' states and therefore on the tunneling probability.

In this paper we numerically study electron tunneling through liquid water confined between two parallel planar electrodes. We consider in some detail the dependence of the tunneling probability on the thickness of the water layers and their structure, and compare the relative roles played by ''bulk'' water molecules and those directly adjacent to the electrode surfaces. We analyze our results in terms of an effective rectangular barrier model characterized by its height and width, taken as independent parameters. In this analysis, we assume that these parameters do not depend on the energy of the tunneling electron, so that its success can be used to assess the adequacy of such one-dimensional models. The results of the numerical calculations reported below suggest that such fits to effective one-dimensional rectangular barriers are successful in many, but not all, situ-

[a]Present and permanent address: Department of Chemistry, University of California, Santa Cruz, 95064.
[b]Present and permanent address: Department of Chemistry, University of New Mexico, Albuquerque, 87131.

ations. Moreover, even when an effective rectangular barrier describes the tunneling successfully, the associated height and width depend on the water structure in the interfacial region. Considerable departure from the rectangular barrier fit is found for structures that support resonance tunneling. The effect of details associated with the electron–barrier interaction is also studied, by comparing results obtained from using two models for this interaction. In the first, the electron–water interaction is taken as a sum of two-body terms, while in the second, the full many-body interaction associated with the water electronic polarizability is taken into account.

This paper is organized as follows: In Sec. II, we describe our model systems and potentials, and briefly discuss the methodology for preparing the water configurations and for calculating the tunneling probabilities. In Sec. III, we analyze and discuss the results of the numerical calculations for different water layers, and consider the suitability of one-dimensional barrier models. Conclusions are presented in Sec. IV.

II. MODEL AND METHODS

The calculation of electron tunneling probability through water layers involves two independent steps. First, we prepare equilibrium configurations of the water molecules between two metal walls using classical molecular dynamics simulations. Next, we solve for the quantum mechanical tunneling through the static configurations. These two steps will be referred to as the classical and quantum parts in the description below.

A. Water–water and water–wall potential energy functions

We choose as our water potential a polarizable flexible simple point charge model (PFSPC), which has recently been used to study the properties of water near the Pt surface.[13] The model represents a modification of a polarizable rigid SPC model developed by Dang, who has demonstrated that this model can reproduce many of the properties of liquid water quite reasonably.[14] Briefly, the intermolecular water potential includes a sum over two-body Lennard-Jones plus Coulomb interactions between the atomic sites and a many-body contribution due to the polarizable nature of the oxygen and hydrogen atoms. This contribution is calculated iteratively to achieve a self-consistent solution for the induced dipoles on the atoms of the water molecules. (For more information, see the discussion on the water–electron potential below.) The intramolecular potential is a polynomial fit to the water vibrational spectra and includes bond stretching, angle bending, and stretch–bend couplings.[15] More information about the potential and its fixed parameters can be found elsewhere.[13,14]

The metal surface is represented by three layers of Pt atoms, each layer being made of 6×6 unit cells of a fcc lattice. The water–metal interaction energy is determined as a sum of the O–Pt and H–Pt pair interactions. These pair interactions are taken from the work of Spohr and Heinzinger.[16,17] They give rise to an interfacial water structure that is consistent with the work function and surface potential measurements. Specifically, the lowest energy state for a single water molecule corresponds to an adsorption of the water with the oxygen on top of a Pt atom with the water dipole oriented away from the surface. When a full water layer is adsorbed, the tendency to maximize hydrogen bonding results in a water dipolar orientation that is mainly parallel to the surface, although a substantial net dipole normal to the interface still remains and causes a reduction in the metal's work function. More details about the potential energy functions and the interfacial water structure can be found elsewhere.[17]

B. Systems preparation

Six different systems are prepared. The first four systems (A–D) include several (1–4, respectively) water layers. Each one of these four systems is prepared by starting from an equilibrated configuration of 500 water molecules between the two parallel Pt(100) surfaces and by removing enough water molecules to leave the desired number of water layers. The metal walls are then moved to new positions consistent with a water density of 1 g/cc. The systems are equilibrated for 200 ps, and the molecular dynamics run continues for an additional 200 ps in order to generate statistically uncorrelated water configurations. Systems F and G are prepared from system B by pulling apart the metal walls with the adsorbed water monolayers on them up to a desired distance. This distance is set equal to the distance in the systems with three and four full layers of water, respectively. This is done in order to gain more insight into the role played by the adsorbed water layer (as will be discussed below). In all cases, the molecular dynamics calculations are done using the Verlet velocity algorithm[18] with an integration time step of 0.5 fs. The self-consistent calculation of the induced dipoles on the water molecules is done every time step with a tolerance of 10^{-4} D, which requires 2–3 iterations to achieve convergence.

The density profiles of the water molecules in systems A–F are shown in panels (a)–(f) of Fig. 1. In all cases, the system's cross section is 23.5 Å$\times$23.5 Å. The layer structure is clearly visible. It must be kept in mind that although these density profiles represent an average over many configurations (sampled during the 200 ps of trajectory), the structure of individual configurations still has the same general characteristic layer structure.

C. Water–electron potentials

The total potential experienced by the tunneling electron is assumed to be a superposition of a rectangular barrier representing the vacuum potential and the water–electron interaction. Two types of the latter interaction are considered in this work. One is the pseudopotential developed by Barnett *et al.*,[19] which will be referred to as the nonpolarizable model, and the other is a polarizable model. The nonpolarizable model is an effective two-body potential and, in addition to the Coulomb, exchange, and exclusion terms, also

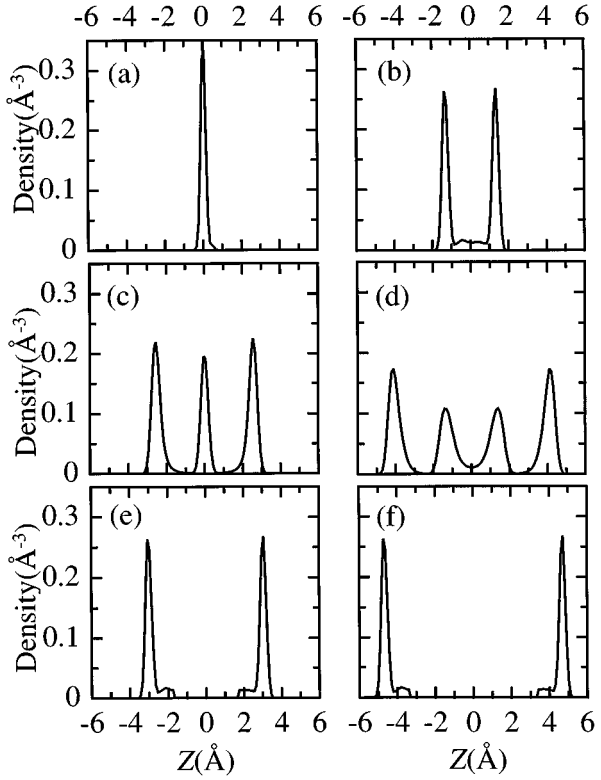

FIG. 1. Density profile of the water oxygens as a function of the distance between two parallel slabs of the Pt(100) surface at $T=300$ K for the six different systems (A–F) described in the text. $Z=0$ is the point midway between the two metal surfaces.

includes a term which takes into account the polarizability of the water molecule in an average way. This is done by taking the corresponding contribution to the electron–water interaction as a sum of the two-body potential of the form,

$$U_p^{\mathrm{NP}}(\mathbf{r})=\sum_j^N -\frac{\frac{1}{2}\alpha e^2}{[|\mathbf{r}-\mathbf{R}_j|^2+\mathbf{R}_c^2]^2}, \tag{1}$$

where $\alpha=1.444$ Å^3, is the effective value of the polarizability determined in Ref. 19, $\mathbf{R}_j$ is the position vector of the oxygen of the jth water molecule, $\mathbf{r}$ is the electron position vector, e is the electron charge, and the sum is over the N water molecules. $R_c=0.85$ Å is a cutoff distance (somewhat arbitrarily selected to be approximately the OH bond distance), which eliminates the zero distance singularity in this interaction. This potential has been used to study electron hydration and hydrated electron spectroscopy.[20] It is similar to other water–electron pairwise pseudopotentials,[21] and it is able to qualitatively account for the general features of electron solvation structure and energetics.

Although the polarizable nature of the water molecule is taken into account in the above model in an approximate way through effective two-body terms, there is evidence that a more accurate treatment of the many-body polarizable nature of the water molecule is necessary in some cases in order to achieve a better quantitative agreement with experiments.[22–24] In particular, we have recently demonstrated that taking into account the many-body aspect of the polarizability contribution to the water–electron interaction significantly affects the computed tunneling probability.[4]

There is no completely satisfactory way to treat the many-body nature of the water–electron interaction, and several approximate schemes have been proposed that could be used depending on the time scale of electron motion.[25,26] Our choice is based on the assumption that the tunneling process is slow relative to the electronic response time of the water molecule, so that the calculations of the water molecules' induced dipoles is done for a fixed position of the electron. Under this assumption, Eq. (1) is replaced by

$$U_p^p(\mathbf{r})=-\tfrac{1}{2}\sum_j^N \boldsymbol{\mu}_j\cdot\mathbf{E}_j, \tag{2}$$

where $\boldsymbol{\mu}_j$ is the electric dipole induced on the jth oxygen, and $\mathbf{E}$ is the electric field due to the electron at the position of the oxygen of the jth water molecule,

$$\mathbf{E}_j=e\,\frac{\hat{r}_j}{\tilde{r}_j^{\,2}}, \tag{3}$$

where $\hat{r}_j$ is a unit vector from the electron to the jth oxygen, and $\tilde{r}_j^{\,2}=|\mathbf{r}-\mathbf{R}_j|^2+R_c^2$. The electric dipoles induced on the water molecules are determined by iterative solutions of the equations,

$$\boldsymbol{\mu}_j=\alpha\left[\mathbf{E}_j-\sum_{k\neq j}^N \mathbf{T}_{jk}\cdot\boldsymbol{\mu}_k\right], \tag{4}$$

where $\mathbf{T}_{jk}=(1/r_{jk}^3)(I-3\hat{r}_{jk}\circ\hat{r}_{jk})$ is the polarizability tensor in which r_{jk} is the distance between oxygens j and k, and $\hat{r}_{jk}$ is a unit vector from oxygen j to oxygen k. More details about this can be found in an earlier publication.[4] We will refer to the model given by Eqs. (2)–(4) as the polarizable model.

Using this procedure for the polarization energy and including the other Coulomb, exchange, and exclusion terms, we determine on a grid of size $16\times16\times200$ the electron–water interaction energy for a static configuration of water molecules. The grid spacing is 1.47 Å in the X and Y directions and 0.211 Å in the Z direction (the direction normal to the metal surfaces). Figure 2 shows the $X-Y$ average of the electron–water potential $U(\mathbf{r})$ in one water configuration for each of the six systems. In each case, the height of the rectangular potential representing the vacuum barrier is taken to be 5 eV. As is clear from Fig. 2, the effect of the water–electron many-body polarizability is to lower the barrier. This lowering is most significant in the high potential energy regions (the peaks) and more modest in the minima. We note that the shape of the one-dimensional averaged potentials mirror the density profiles shown in Fig. 1, a reflection of the hard-core electron–oxygen repulsion. However, one must keep in mind that the one-dimensional potentials shown in Fig. 2 may be misleading because the three-dimensional tunneling electron will most likely avoid the high potential energy regions associated with the oxygen cores.

Some information about the lateral structure of the water layers is given in Fig. 3, where the projected $X-Y$ distribution of the oxygen positions for one configuration of the

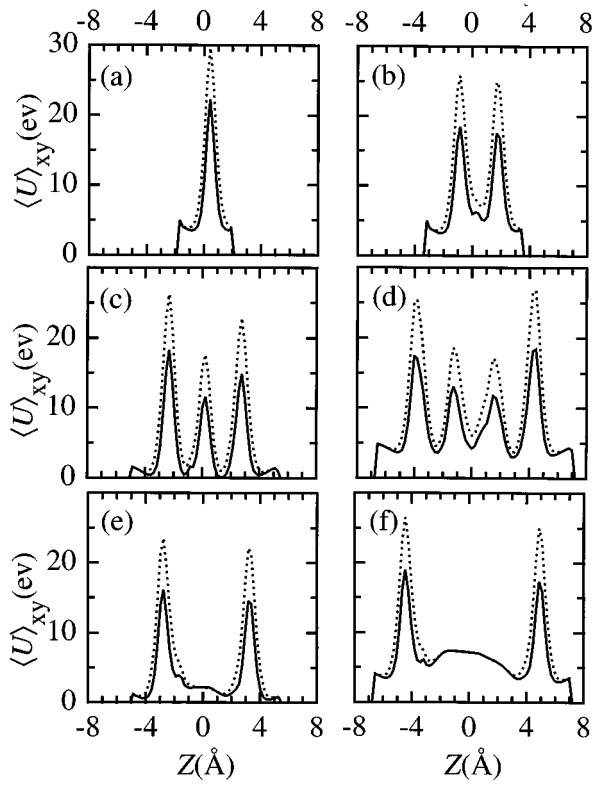

FIG. 2. The $X-Y$ average of the water–electron potential energy as a function of the distance between the metal surfaces. Each panel represents the potential evaluated from one water configuration for a system whose corresponding density profile appears in Fig. 1. In each panel, the solid line corresponds to the many-body polarizable model, and the dotted line gives the potential evaluated using the nonpolarizable water-electron potential. Each potential energy curve includes the bare (vacuum) barrier of 5 eV.

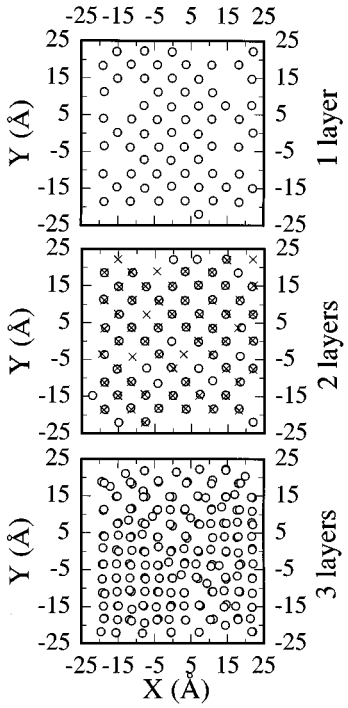

FIG. 3. Projected (onto the XY plane) positions of the water oxygens for a single configuration of the one-, two-, and three-layer water systems. In the center panel, the ''○'' and ''×'' designate the oxygens in the two different layers.

one-layer, two-layer, and three-layer systems is depicted. It is useful to analyze these structures in terms of the projected two-dimensional density of oxygen cores. We note that there is considerable cubic symmetry ordering, which reflects the underlying symmetry of the Pt(100) surface. However, because this cubic structure is incompatible with the water hydrogen bonding structure, there are defects and some disorder in the structure.[17,27] These defects constitute ''holes'' in the one-layer structure. In the two-layer system these holes are filled, but most of the oxygen cores lie directly behind each other along the direction normal to the walls, and therefore the projected two-dimensional density is largely unchanged. In the three-layer system, the additional oxygen cores are situated in between the oxygens of the first two layers, which results in a marked increase in the projected two-dimensional density. Since the electron is unlikely to go through the oxygen cores, one may expect (if the tunneling is dominated by straight paths connecting the metal walls in the normal direction) that the transmission probability will be inversely correlated with the projected two-dimensional density of the oxygen cores and therefore significantly reduced in the three-layer case relative to the one- and two-layer systems (for the same distance between the metal walls). We see below, when we discuss the effective barrier for the electron tunneling, that the actual situation is more complicated.

D. Numerical calculation of the tunneling probabilities

In our previous calculations of tunneling probabilities through water layers, we have used the time-dependent wave packet propagation method.[3,28] This method can become highly inefficient when the thickness of the water layer increases beyond three layers, in particular when there are long-lived resonance states in the system which result in temporal trapping of the wave packet. Thus, a new approach based on the absorption boundary conditions Green's function method is used here.[29] Briefly, the Hamiltonian for the single electron moving in the potential $U(\mathbf{r})$ is represented on the $16\times16\times200$ cubic grid using a seventh-order finite difference representation of the kinetic energy operator.[29,30] The total tunneling probability for an electron with a given initial energy E moving along the Z direction (normal to the interface) is calculated by sparse matrix diagonalization techniques.[31,32] Thus, what we calculate is

$$P(E)=\sum_f |S_{if}(E)|^2, \tag{5}$$

where $S_{if}(E)$ is the scattering matrix for the transition from the free electron state $\mathbf{k}_i$ to the free electron state $\mathbf{k}_f$ and $\hbar^2k_i^2/2m_e=\hbar^2k_f^2/2m_e=E$, $\mathbf{k}_i=k_i\hat{z}$. We emphasize that this is done for a static configuration of water molecules.

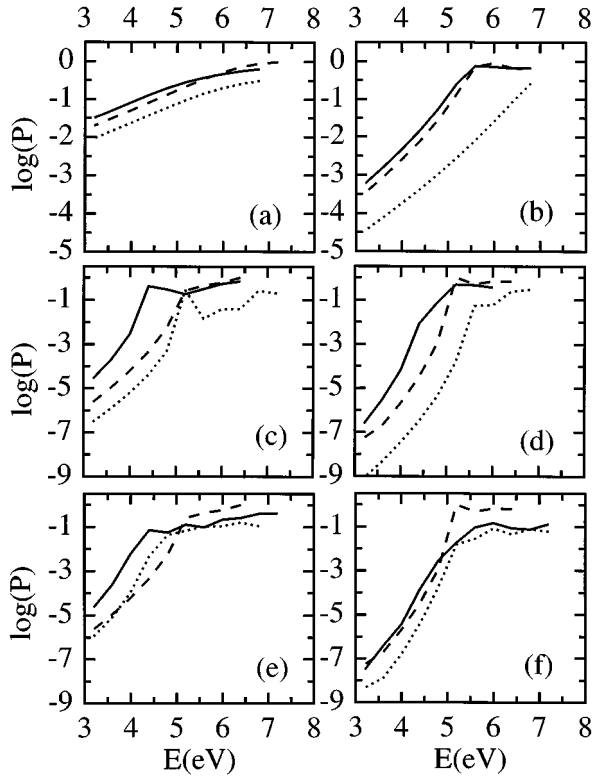

FIG. 4. Electron transmission probability as a function of incident energy for systems A–F (panel locations same as in Figs. 1 and 2). In each panel, the solid line corresponds to the many-body polarizable water–electron potential, the dotted line to the nonpolarizable potential, and the dashed line to the bare rectangular barrier.

III. RESULTS AND DISCUSSION

Figure 4 summarizes the results of the transmission probability through one configuration of each of the six systems, using the polarizable and nonpolarizable potentials. Also shown are the transmission probabilities through the corresponding bare barriers. (The bare barrier results are obtained numerically in order to test the accuracy of the program. They are very close to the results of the analytical formula given below.) We first discuss the low energy results ($E \leqslant 4.4$ eV) and then consider the transmission of electrons with near- and overbare barrier energies.

As can be seen from the low energy region of panels (a)–(d) of Fig. 4, the tunneling probability is approximately exponential in energy for $E \leqslant 4.4$ eV. For this energy range, the tunneling probability calculated with the polarizable model is always greater than the one calculated with the nonpolarizable model. The latter is even lower than the tunneling probability through the bare 5 eV rectangular barrier: $P_P(E) > P_{\mathrm{vac}}(E) > P_{\mathrm{NP}}(E)$. The contribution of the many-body water–electron polarizability to the enhancement of the tunneling rate has been shown in previous calculations (with three layers of water) to be the result of a lower barrier and more extended electron states. This effect seems to be getting larger as the number of water layers increases.

Because of the prominent role played by one-dimensional models in the fitting of experimental tunneling results, it is of interest to analyze the numerical results of the low energy tunneling in terms of an equivalent one-dimensional rectangular barrier, for which[33]

$$P = \frac{1}{1 + \dfrac{U_b^2}{4E(U_b - E)} \sinh^2 \sqrt{\dfrac{U_b - E}{3.811}}\, L}, \tag{6}$$

where E and U_b are the electron's energy and the barrier height in electron volts, respectively, and L is the barrier width in angstroms. Note that this formula also applies to over-barrier transmission, using the identity $\sinh^2 \sqrt{-x} = -\sin^2 \sqrt{x}$.

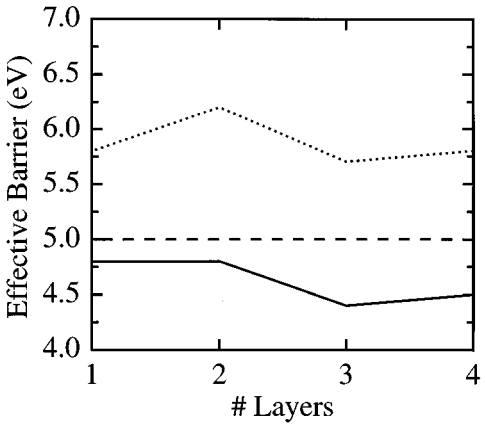

FIG. 5. The effective one-dimensional barrier obtained by fitting the low energy tunneling probability to the analytical results for tunneling through a rectangular barrier. Solid, dotted, and dashed lines correspond to the polarizable, nonpolarizable, and bare barrier potentials, respectively.

The effective one-dimensional barrier height, U_b, obtained from fitting the numerical results to Eq. (6), is shown in Fig. 5 as a function of the number of water layers. (The barrier width is set equal to the actual width in each case. These widths are given in Table I below.) We first note that, as expected, the effective barrier height for the polarizable case is lower than that of the vacuum (by about 0.3–0.6 eV), and the effective barrier height for the nonpolarizable case is greater than that of the bare barrier (by about 0.5–1.2 eV). The effective barrier height depends on the number of water layers, thus showing that the one-dimensional model is not very accurate. In particular, we note the lower effective barrier in the three-layer case, despite the fact that the structure seems to be much more blocked (Fig. 3). However, the quality of the fit, as judged by the root mean square deviation of the numerical results from the analytical formula, is quite good, except for the three-layer case (Table I). This suggests that the one-dimensional model, despite being physically inaccurate, can provide a reasonable qualitative description in some, but not all (see the discussion on over-barrier results below) cases. We also mention that a two-parameter fit of the low energy results, in which both the barrier height and barrier width are allowed to vary, gives a somewhat better fit (but again, not for the three-layer case). The resulting effective barrier height is almost the same as in the one-parameter fit, and the width is always larger than the actual width.

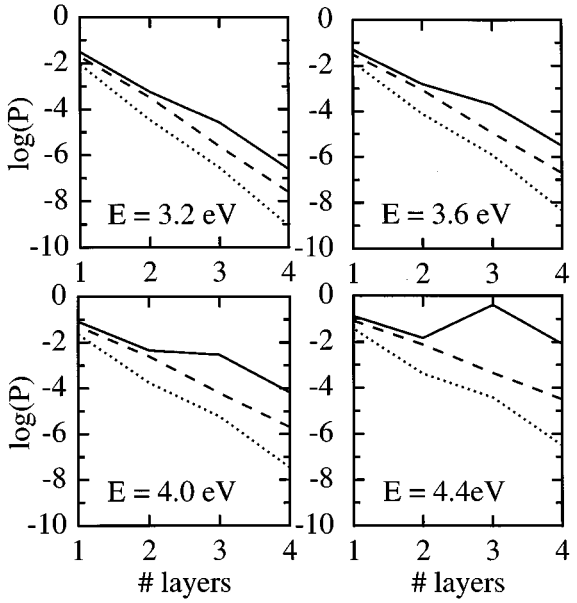

FIG. 6. Electron transmission probability as a function of the number of water layers at different incident energies. Solid, dotted, and dashed lines correspond to the polarizable, nonpolarizable, and the bare barrier potentials, respectively.

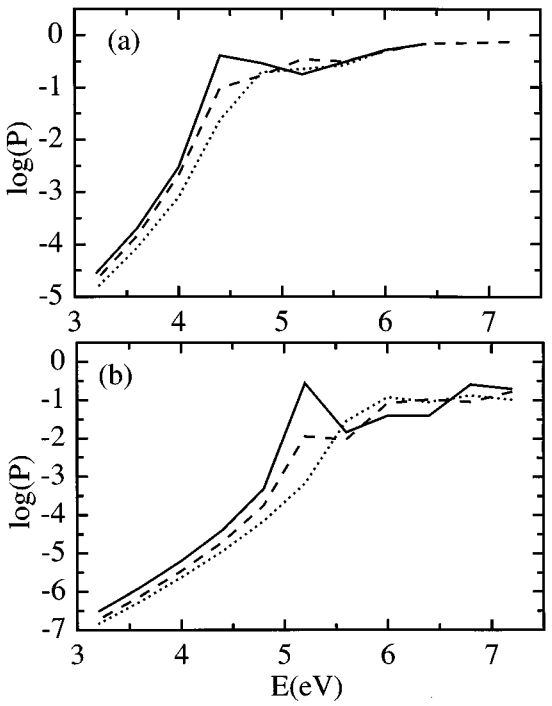

FIG. 7. Electron transmission probability as a function of electron energy for tunneling through three layers of water. Panels (a) and (b) correspond to the polarizable and nonpolarizable models, respectively. The solid lines represent the same data as in panel 4(c). The dashed and dotted lines correspond to different water configurations separated from the first one by 50 and 100 ps, respectively.

The dependence of the tunneling probability on the number of water layers is shown in Fig. 6. We note that the near exponential behavior at the lowest energy is significantly distorted as one reaches the 4.4 eV electron energy because of the anomalously high tunneling probability through the three-layer case. This behavior is consistent with the dip in the effective barrier and the poor fit to the one-dimensional model mentioned earlier, and it suggests that the three-layer system supports a resonance state. An examination of the higher energy results [the solid line Fig. 4(c)] shows that there is a broad peak in the transmission probability near $E=4.4$ eV and an even more significant peak (shifted to the higher energy of 5.2 eV) when one utilizes the nonpolarizable model but the same water configuration [the dotted line Fig. 4(c)]. This suggests that the existence of the resonance state is a manifestation of the water structure, and only its location on the energy scale is sensitive to the choice of the potential energy function.

If the resonance state is the result of a specific water configuration, then one would expect it to disappear or shift in energy as the positions of the water molecules change. A hint that this is indeed the case is provided in Fig. 7, which shows the results of the tunneling calculations in two additional water configurations separated by 50 and 100 ps from the configuration discussed above. One notes that for energies both lower and higher than the presumed location of the resonance, the transmission probabilities for the three configurations are quite close, but as one reaches this region, significant deviation can be seen. In particular, the large peak in the nonpolarizable case completely disappears.

In order to better evaluate the suitability of the one-dimensional tunneling model, one must examine all of the energy ranges both below and above the bare barrier. We find that whereas the low energy results can be reasonably fitted to a one-dimensional rectangular barrier model, as is evident in the data given in Table I, the fit to the whole energy range is very poor (and does not improve significantly when both the barrier width and height are allowed to vary). This is demonstrated in Fig. 8, where we show the best fit to the numerical results for two water configurations of the three-layer case, for both the polarizable and nonpolarizable models.

Molecular dynamics studies of the structure of water at metal interfaces[17,34] reveal that the first water layer near the surface has a unique orientational structure with a relatively high degree of order. There is a substantial potential drop

TABLE I. Effective barrier height for the different water layers.

Number of water layers	Effective barrier (eV)		Barrier width (Å)	Number of water molecules
	Polarizable	Nonpolarizable		
1	4.8(0.012[a])	5.8(0.03)	3.6	63
2	4.8(0.012)	6.2(0.009)	6.6	130
3	4.4(0.16)	5.7(0.12)	10.0	197
4	4.5(0.28)	5.8(0.12)	13.3	257
2/3[b]	4.4(0.32)	5.0(0.54)	10.0	130
2/4[c]	4.9(0.22)	5.5(0.28)	13.3	130

[a]The root mean square deviation of the fitted log probabilities from the numerical values.
[b]Two layers of water in the space of three layers.
[c]Two layers of water in the space of four layers.

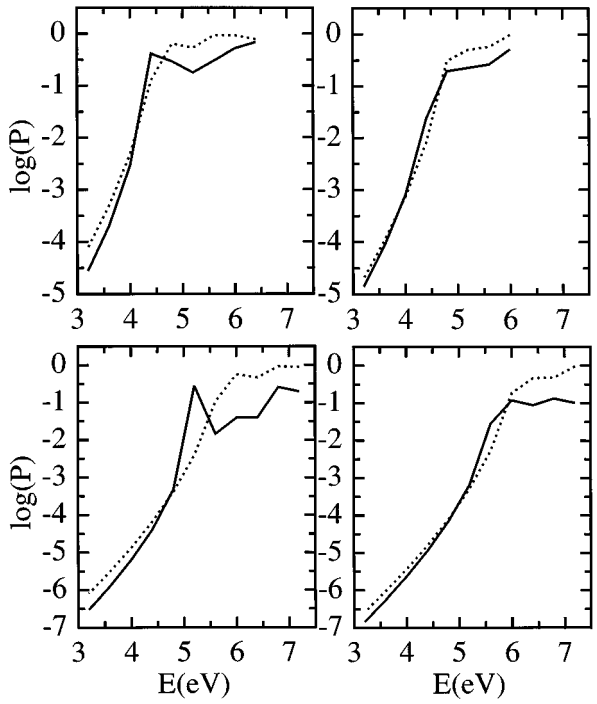

FIG. 8. A comparison of numerical and fitted data over the entire energy range for electron transmission through three layers of water. In each panel, the solid line gives the numerical results and the dotted line the best fit to Eq. (6). The top two panels correspond to the two water configurations that are separated by 100 ps and using the polarizable model, and the bottom two panels are the same two configurations using the nonpolarizable model.

across the interface, which results in lowering the work function of the metal. Some insight into the role of the first layer of water is provided by our studies of systems E and F, in which the two metal walls with the adsorbed water monolayers are separated by empty space so that the total width is the same as the full three and four layers of water, respectively. As can be seen from Table I, the effective barrier in the polarizable two layers in the space of three (system E) is equal to the effective barrier in the three-layer system, suggesting that the middle water layer does little to change the tunneling probability. It is likely that competing effects are at work here. The middle layer of water in the three-layer case is translationally disordered and decreases the probability of electron tunneling by the blocking oxygen cores (see Fig. 3). At the same time, the additional water molecules lower the peak of the potential energy so that the end result is that the tunneling probabilities through the three-layer system (system C) and through system E are quite similar. Another interesting feature emerging from the comparison of Figs. 4(c) and 4(e) is that the pronounced peak in the full-layer case (which is especially evident in the nonpolarizable model) disappears when the middle layer of water is removed. This could suggest that the resonance state involves water molecules in the middle layer. However, one needs to compute the wave function associated with the electronic state in the system in order to support this suggestion.

The contribution of the bulk water polarizability to lowering the energy seems to be more important than the blocking effect in the four-layer case as is evident from the fact that the effective barrier in system F (two layers in the space of four) is greater than that in system D (four water layers). We thus conclude that although the adsorbed layers of water near the metal surface are the most important for a quantitative account of the tunneling process, the role played by bulklike water polarizability and the three-dimensional structure of the oxygen cores is also significant.

IV. SUMMARY AND CONCLUSIONS

Using the absorbing boundary condition Green function method, we have calculated the transmission probability of an electron through water layers of varying thickness over a wide energy range, using both polarizable and nonpolarizable water–electron potentials.

Although we believe that our general conclusions are valid for realistic electron tunneling through water structures, our model includes some simplifying assumptions that prohibit a quantitative comparison with experiments. First, we are limited by the models used for the electron–water, electron–metal, and water–metal potentials. Although significant progress has been made in recent years in the development of water–electron pseudopotentials,[19,21,26] such potentials should be viewed as highly empirical. In particular, the electron–water pseudopotential describes the charge transfer as a single electron process and disregards possible contribution of hole transfer.[35] Second, we only consider static water structures, assuming that the water nuclear motion is slow on the time scale of the tunneling process. This assumption is usually valid for nonresonance tunneling processes, but is questionable when the tunneling is dominated by barrier resonances. Because of numerical constraints, we are limited to relatively thin water films that are difficult to characterize and to study experimentally. In addition, we consider only electrons incident in the direction perpendicular to the film (instead of averaging over an appropriate Fermi distribution of energies and over all incident directions). Third, limited computational resources force us to examine only a small number of configurations, i.e., an averaging ensemble which may be too small. Thus, if the tunneling process is dominated by rare molecular configurations, our calculations may underestimate the tunneling probability by missing these configurations in our limited ensemble. We would like to point out that an examination of a larger number of configurations in the three-layer case showed a relatively small scatter in the data.[3] The tunneling pathways may still be dominated by rare structures, but one first needs to identify these structures in order to estimate their probability. Finally, because of the computational limitation on the size of the Hamiltonian matrix, the grid spacing in the directions parallel to the layers may be too coarse. This could result in some details of the electron–water potential being missed which could affect the tunneling pathway.

Even with these drawbacks, we are able to gain a substantial understanding of the factors which affect electron tunneling through water. In general, the results demonstrate

the inadequacy of one-dimensional tunneling models and the importance of treating the molecular structure of the medium. Although low energy under-barrier tunneling probabilities can be fitted to an effective one-dimensional rectangular barrier model as long as one is far from a resonance state, the full energy range (including near and over-barrier transmission) is not well described using the one-dimensional model.

We find that in all the systems studied, the water many-body electronic polarizability makes an important contribution to the electron–water potential energy and significantly affects the tunneling probabilities. In particular, in the fully polarizable model, the effective barrier is lower than the bare barrier; the observed lowering of 0.5 eV suggests the incipient development of the ''conduction band'' of water ($V_0 \approx 1$ eV) in bulk water.

Finally, we find that the transmission probability is in some cases strongly affected by resonance tunneling, however, the nature of the underlying resonance states and their relative importance is a topic for future studies.

ACKNOWLEDGMENTS

This research has been supported by the U.S.A.–Israel Binational Science Foundation, the Israel Ministry of Science (A.N.), and the U.S.A. National Science Foundation (I.B.). A.N. thanks Professor Marshal Newton for very useful discussions and correspondence.

[1] A. M. Kuznetsov, *Charge Transfer in Physics, Chemistry and Biology* (Gordon and Breach, Amsterdam, 1995).
[2] W. Schmickler, Surf. Sci. **335**, 416 (1995).
[3] A. Mosyak, A. Nitzan, and R. Kosloff, J. Chem. Phys. **104**, 1549 (1996).
[4] A. Mosyak, P. Graf, I. Benjamin, and A. Nitzan, J. Phys. Chem. (in press).
[5] K. A. Motakabbir and P. J. Rossky, Chem. Phys. **129**, 253 (1989).
[6] J. Halbritter, G. Repphun, S. Vinzelberg, G. Staikov, and W. J. Lorentz, Electrochim. Acta **40**, 1385 (1995).
[7] G. Repphun and J. Halbritter, J. Vac. Sci. Technol. A **13**, 1693 (1995).
[8] A. Vaught, T. W. Jing, and S. M. Lindsay, Chem. Phys. Lett. **236**, 306 (1995).
[9] U. Mazur and K. W. Hipps, J. Phys. Chem. **99**, 6684 (1995).
[10] N. J. Tao, Phys. Rev. Lett. **76**, 4066 (1996).
[11] L. Sanche, Scanning Microsc. **9**, 619 (1995).
[12] A. Haran, A. Kadyshevitch, H. Cohen, R. Naaman, D. Evans, T. Seidman, and A. Nitzan, (unpublished).
[13] I. Benjamin (unpublished).
[14] L. X. Dang, J. Chem. Phys. **97**, 2659 (1992).
[15] K. Kuchitsu and Y. Morino, Bull. Chem. Soc. Jpn. **38**, 814 (1965).
[16] E. Spohr and K. Heinzinger, Ber. Bunsen-Ges. Phys. Chem. **92**, 1358 (1988).
[17] E. Spohr, J. Phys. Chem. **93**, 6171 (1989).
[18] M. P. Allen and D. J. Tildesley, *Computer Simulation of Liquids* (Clarendon, Oxford, 1987).
[19] R. N. Barnett, U. Landman, and C. L. Cleveland, J. Chem. Phys. **88**, 4420 (1988).
[20] R. N. Barnett, U. Landman, and A. Nitzan, J. Chem. Phys. **89**, 2242 (1988).
[21] P. J. Rossky and J. Schnitker, J. Phys. Chem. **92**, 4277 (1988).
[22] M. Sprik, M. L. Klein, and K. Watanabe, J. Phys. Chem. **94**, 6483 (1990).
[23] L. X. Dang, J. E. Rice, J. Caldwell, and P. A. Kollman, J. Am. Chem. Soc. **113**, 2481 (1991).
[24] G. Markovich, L. Perera, M. L. Berkowitz, and O. Cheshnovsky, J. Chem. Phys. **105**, 2675 (1996).
[25] J. Cao and B. J. Berne, J. Chem. Phys. **99**, 2902 (1993).
[26] A. Staib and D. Borgis, J. Chem. Phys. **103**, 2642 (1995).
[27] K. Raghavan, K. Foster, and M. Berkowitz, Chem. Phys. Lett. **177**, 426 (1991).
[28] H. Tal-Ezer and R. Kosloff, J. Chem. Phys. **81**, 3967 (1984).
[29] T. Seideman and W. H. Miller, J. Chem. Phys. **96**, 4412 (1992).
[30] J. C. Light, I. P. Hamilton, and J. V. Lill, J. Chem. Phys. **82**, 1400 (1985).
[31] Y. Saad, *Iterative Methods for Sparse Linear Systems* (PWS, Boston, 1996).
[32] D. Evans, T. Seidman, H. Tal-Ezer, and A. Nitzan (unpublished).
[33] L. D. Landau and E. M. Lifshitz, *Quantum Mechanics: Non-relativistic Theory* (Pergamon, New York, 1977).
[34] K. Raghavan, K. Foster, K. Motakabbir, and M. Berkowitz, J. Chem. Phys. **94**, 2110 (1991).
[35] We thank Professor M. Newton for bringing up this point.